scientific reports



OPEN

Simultaneous measurement of liquid level and R.I. sensor using POF based on twisted structure

Muhammad Saleh Urf Kumail Haider¹, Chen Chen¹, Abdul Ghaffar¹, Sadam Hussain³, Mujahid Mehdi⁴, Laraib Unsa Noor², Sabir Ali Kalhoro⁵ & Min Liu¹

In this paper, a dual-parameter liquid level and refractive index (R.I.) sensor is fabricated using three pieces of bare polymer optical fibers (POFs), which can independently and simultaneously sense the liquid level and R.I. The proposed sensor design utilizes the twisted coupling technique, in which two optical fibers are twisted and coupled with macro-bending. The liquid level measurement depends on the coupling loss, where the light is transmitted to emission fiber (EF) and twisted with coupled acceptor fiber (AF). The proposed liquid level sensor can measure depths up to 125 mm with a sensitivity of 8.03 nW/mm. Moreover, R.I. sensing depends on the twisted coupled macro-bending (TCMB) technique, where the EF generates bend loss and the AF couples the loss, where the coupled power varies due to the transformation in R.I. of coupling medium. The R.I. sensor revealing a notable sensitivity of -2663%/RIU and an impressive resolution of 3.754×10⁻⁴ in the different NaCl-saturated liquids featuring R.I. range extending from 1.333 to 1.361. The experimental findings indicate the sensor exhibits excellent stability and reliability. The sensor's straightforward, comprehensive, and cost-effective design enables its application in chemical, petroleum, and other industries.

Keywords Liquid level sensor, R.I. sensor, Multi parameter technique, Coupling, Bend loss

The simultaneous multiparameter sensing technique has become essential in several scientific and industrial fields because it allows real-time monitoring, and various multiple parameters can be integrated into a single system. This approach simplifies the monitoring procedure, reduces complexity, and lowers the costs associated with deploying multiple sensors¹. There have been significant advancements in multiparameter sensing applications across various fields, including biological sensing², temperature³, strain measurement⁴, pH detection⁵, liquid level monitoring⁶, soil-nailing⁷ and bend or torque measurement evaluation^{8,9}. The capability to simultaneously measure multiple parameters in real-time, referred to as simultaneous measurement sensing, has received less attention and development compared to these other applications.

Liquid level and refractive index (RI) are crucial across scientific and industrial domains. R.I. sensor investigates liquid composition and optical properties, offering insights about changes in solution concentrations and chemical composition. Multiparameter sensing technique can achieve a deeper understanding of fluid dynamics, mixing processes, and changes in composition. This has the potential to drive innovation across multiple sectors such as chemical processing, pharmaceuticals, and environmental monitoring.

Fiber-based liquid level and R.I. sensors can be categorized according to their underlying measurement principles. Among different methods, the various interferometer techniques used for sensing include Fabry-Perot interferometers (FPI)¹¹, multimode interferometers¹², and Mach-Zehnder interferometers (MZI)¹³, long-period gratings (LPG)¹⁴, and fiber Bragg gratings (FBG)¹⁵, which depend on wavelength modulation and rely on the wavelength of light as the liquid level or R.I. changes. The wavelength modulation technique is more complex and requires more advanced measuring equipment^{16,17}. Despite the fact that the intensity modulation utilizes light intensity, it changes as the liquid level, or R.I., varies^{18,19}. These intensity modulation-based sensors are easier to implement because of their simple and straightforward measurement method. Therefore, intensity modulation-based optical fiber sensors (OFS) are currently the most widely used for liquid level sensing.

¹School of Microelectronics and Communication Engineering, Chongqing University, Chongqing 400044, China. ²College of Mechanical and Vehicle Engineering, Chongqing University, Chongqing 400044, China. ³Key Laboratory of Air-Driven Equipment Technology of Zhejiang Province, College of Mechanical Engineering, Quzhou University, Quzhou 32400, Zhejiang, China. ⁴Aror University of Art Architecture Design & Heritage Sindh, Faculty of Design, Aror, Pakistan, Sukkur, Sindh 65200, Pakistan. ⁵North Dakota State University, Fargo, ND, USA. [™]email: c.chen@cqu.edu.cn; qhaffar@qzc.edu.cn

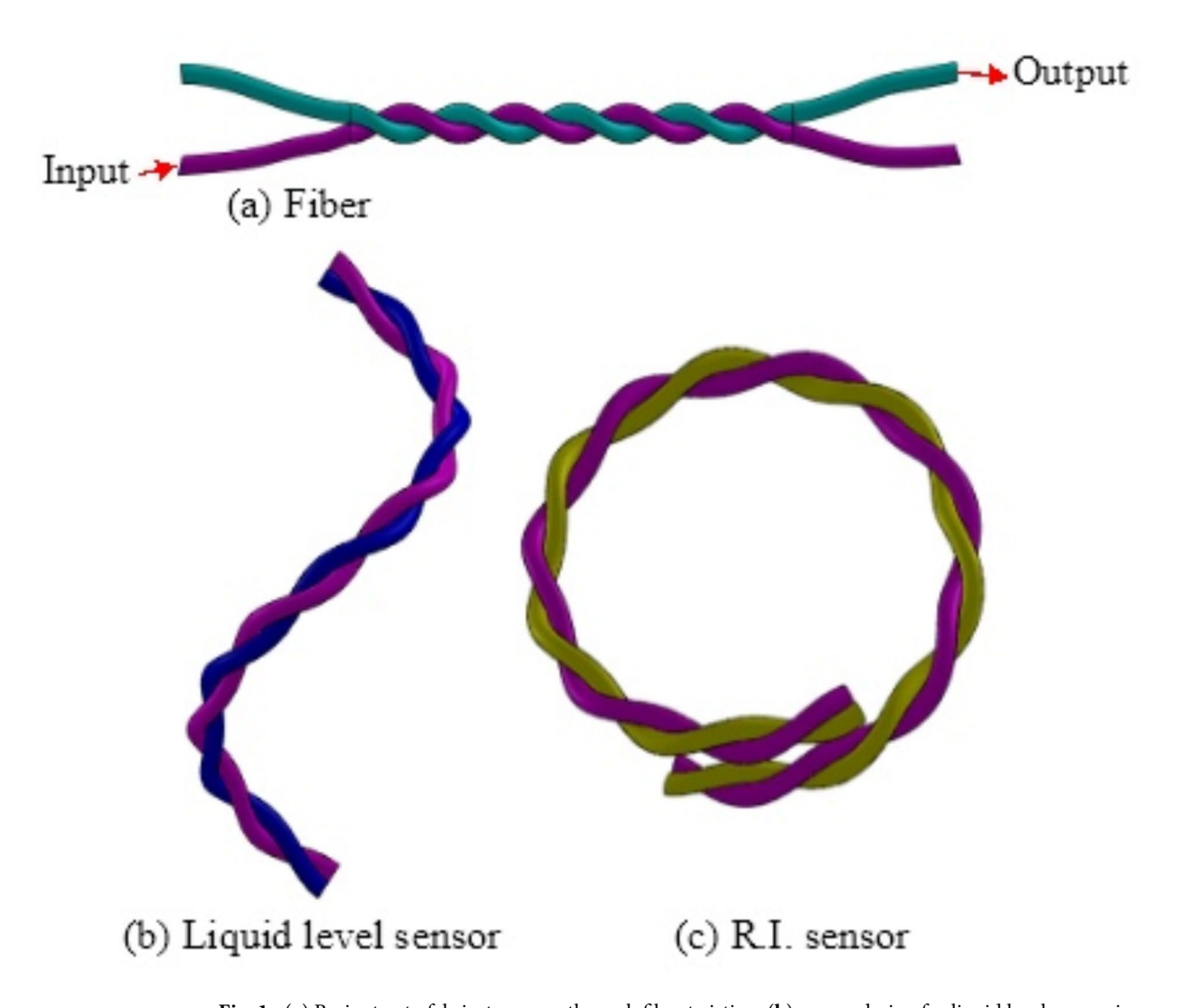


Fig. 1. (a) Basic step to fabricate sensor through fiber twisting, (b) sensor design for liquid level measuring and (c) is R.I. sensor design using TCMB technique.

Polymer optical fiber (POF) offers more advantages compared to silica fiber^{3,20,21}. Numerous studies have improved techniques for measuring liquid level sensing. For example, Dong et al.²² fabricated a model interferometer using a coreless D-shape fiber for liquid level sensing. Zhang et al.²³ fabricated a liquid level sensor that can only sense depth at different points using the coupling method. Another study proposed drilling microholes in the POF for liquid level sensing²⁴. While Deng et al.²⁵ presented an approach for continuous liquid level sensing, they also used twisted tapered POFs. Liquid level can be measured by changing the coupling ratio with respect to the variation of visible light intensity at two different nodes. Moreover, the effects of temperature, R.I., and diameters of POF are analyzed.

A number of sensors have been proposed using various techniques in the literature to measure the liquid level and R.I. For instance, a R.I. measuring technique based on a fiber ring laser utilizing a dual-FBG filter. The fabrication of FBG filters was achieved with a combination of normal FBG and thinned FBG grating. Ujihara et al.²⁶ manufactured a tapered graded index per fluorinated POF by employing intense illumination propagation inside fiber to create a R.I. sensor. Chen et al.²⁷ describe an optical fiber liquid level sensor that fixes R.I. by cascading double multi-mode interferences with photonic crystal fiber and no core fiber. This method integrates a liquid level sensor and a R.I. sensor, utilizing the first for detection and the second for R.I. compensation. However, the cascading of multiple fibers introduces complexities in terms of manufacturing, alignment, and stability. Ning et al.²⁸ introduced a POF-based R.I. sensing probe from commercial POF by macro-bending effect and side-polished it for R.I. measurement. The thermal heating method was used to achieve the micro-bending structure of the POFs. De-Jun et al.²⁹ fabricated the D-shaped POF sensor, which uses a side-half-polishing method for R.I. sensing. The influence of the surrounding environment and the evanescent wave generated by the propagating light causes a reduction in optical transmission, which forms the basis of this operating principle.

Another idea was put forward: Teng et al.³⁰ proposed a POF-based SPR sensing system for simultaneous assessment of R.I. and liquid level. Similarly, Yang et al.³¹ proposed a liquid level and R.I. sensor using MZI

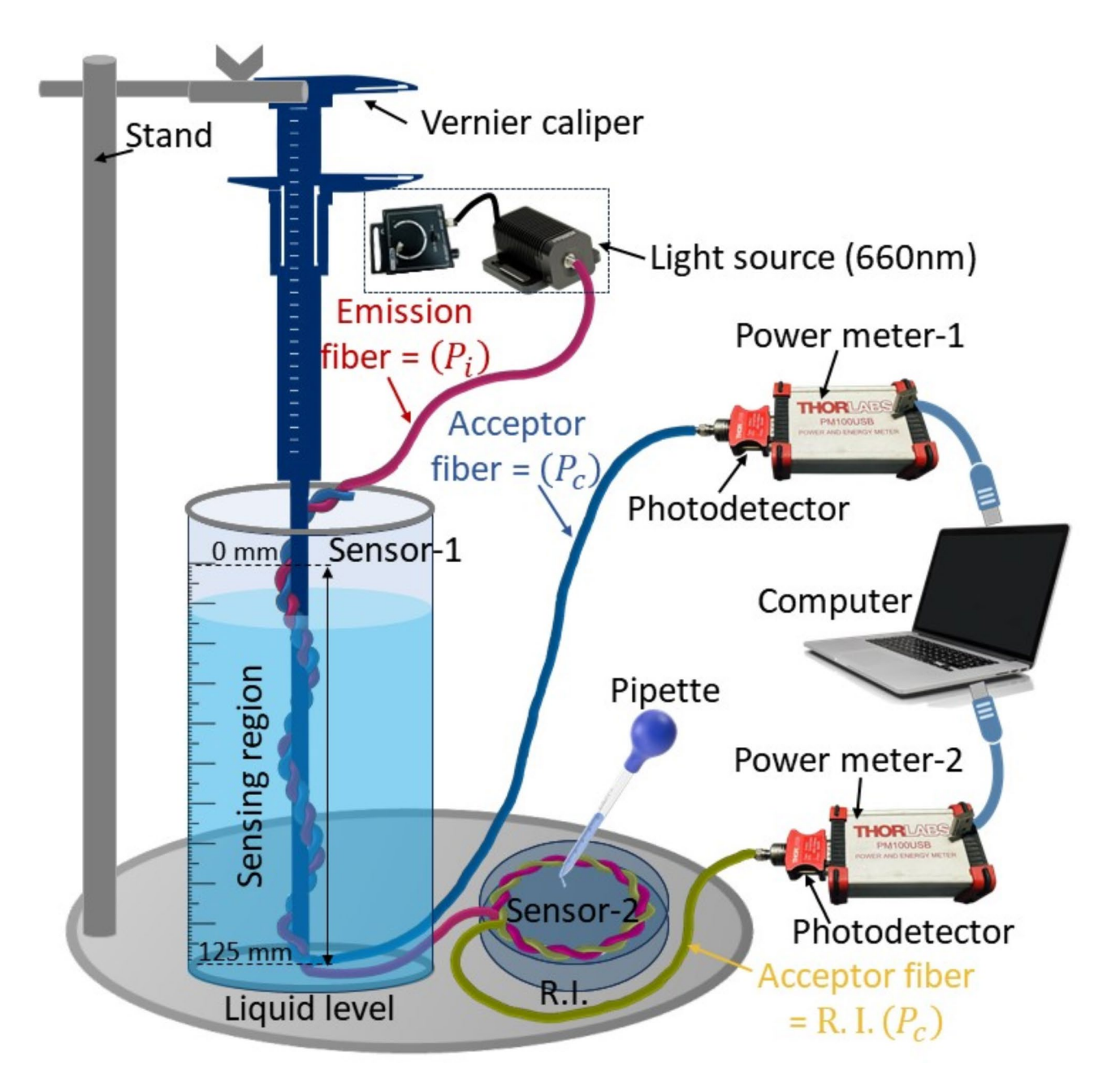


Fig. 2. The schematic drawing of experimental setup.

design utilizing a graded-index multimode fiber (GIMMF) sandwiched between the single-mode fibers and multi-mode fibers. However, the necessity to adjust the length of the GIMMF every time for liquid level measurement hints that the sensor might not be ideal for continuous or real-time monitoring applications. The POF-based surface plasmon resonance (SPR) sensor, featuring a side-polished and V-shaped groove structure, for the multiparameter sensing of R.I. and temperature was also purposed this approach was more cost-efficient than the other purpose multiparameter sensor³². While these side polishing, multiple notches, and micro-hole drilling in the POF are also proposed for multiparameter sensing of liquid level and R.I^{33,34}. However, drilling holes, notches, or V-grooves in POF creates imperfection, vulnerability, and more scattering loss for intensity-based sensors. They also add complexity to the setup, limiting their ability to provide high-resolution and precise measurements. Therefore, there is ongoing research and development in the field of multiparameter sensing of liquid level and R.I., with a focus on improving accuracy, response and high-resolution measurements.

In this paper, we propose an OFS for simultaneous measurement of liquid level and R.I. This sensor is based on the twisted-coupled fiber technique for liquid level sensing, along with the twisted-coupled macro-bending (TCMB) techniques used for R.I. sensing with a single LED source. The sensor structure utilizes three pieces of POFs: one fiber attached to the light source, and the remaining two fibers for liquid level and R.I. sensing. This technique is low-cost and easy to implement, making it suitable for various applications where multiparameter

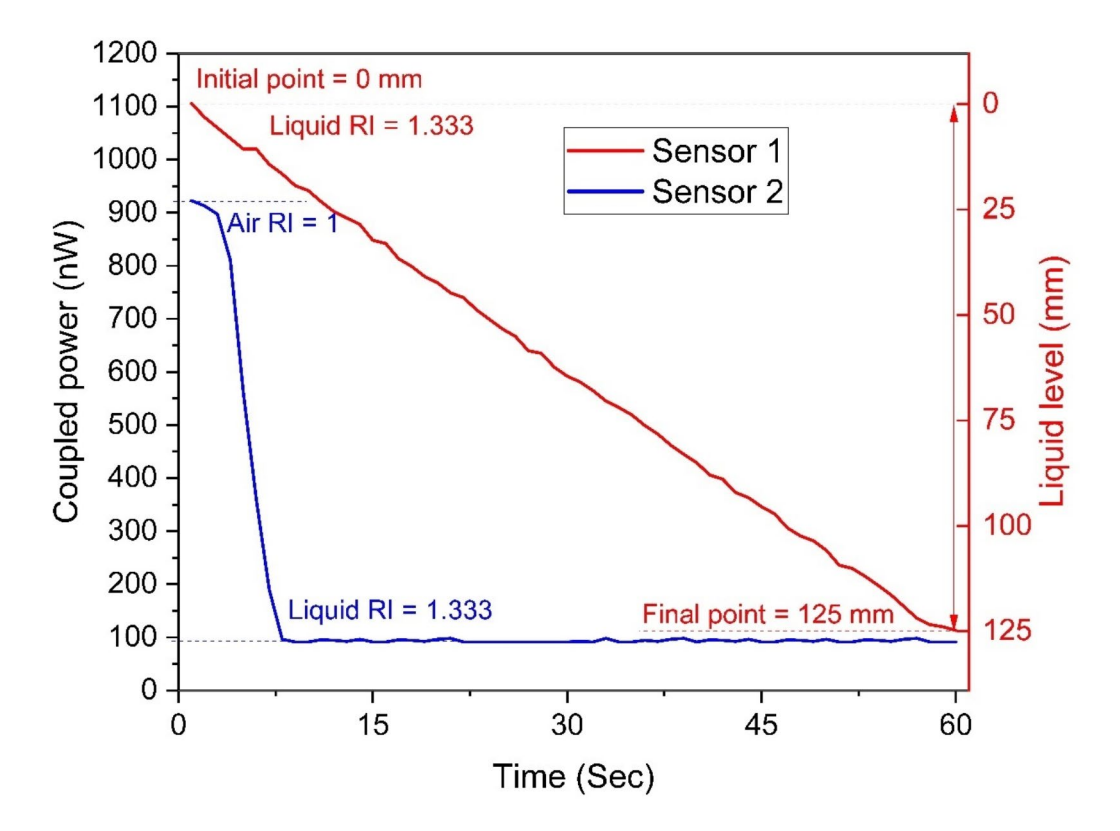


Fig. 3. Initial and final response of liquid level and R.I. sensor in liquid (RI = 1.333).

sensing of liquid level and R.I. is required. Sensor fabrication and sensing phenomena are explained in the next section, whereas the experimental results and their analysis are provided in the fourth section.

Sensor fabrication and sensing principles Twisted coupled and TCMB technique

The proposed design for simultaneous measurement of liquid level and R.I. employs a method involving twisting structures using POFs. In this setup, one fiber responsible for propagating light is attached to the LED source, which is designated the emission fiber (EF). The remaining two fibers operate as acceptor fibers (AFs), each with a unique function. The first AF is twisted with the EF, and this twisting action forms the basis for detecting changes in the liquid level. Essentially, the amount of light transferred between these fibers varies depending on the liquid's height, thus enabling liquid level measurement.

Concurrently, the second AF undergoes a dual treatment of twisting and being subjected to macro-bending. This specific manipulation enables the fiber to demonstrate sensitivity towards variations in the R.I. of the surrounding medium. When the R.I. varies, so does the light transmission pattern between the EF and this second AF, allowing for R.I. measurement. Figure 1a depicts the method of twisting, and twisted coupled fiber for liquid level sensing is shown in Fig. 1b, while Fig. 1c demonstrates TCMB technique in coupled fibers for R.I. sensing. However, to perform the dual sensing tasks, the arrangement and functioning of this sensing system are visually represented in Fig. 2, providing a clear illustration of the fibers that are configured and interact. The liquid level and R.I. sensors both utilize a twisting rate of 1 complete twist every 2 cm. This rate was chosen to balance the light coupling effect between the fibers, ensuring effective power transfer for optimal sensitivity and performance in both sensing applications.

TCMB technique for R.I. sensing

The proposed technique for fabricating a simultaneous measurement sensor capable of detecting dual parameters with a single light source is based on the TCMB loss technique. This allows optical power coupling to detect R.I. changes. This technique employs a twisting and coupling method to enable the coupling of the radiated power from the EF, and then transmit this to the AF for R.I. measurement. Where the EF generates bend loss and the AF couples the loss, this makes the R.I. sensor more sensitive to sense different refractive indices. It is widely accepted that if the cores of two closely spaced fibers are close to one another, light in those fibers will become optically coupled 35. As light propagates through the twisted EF, some of it is lost due to the induced bend. This lost light is then coupled into the AF, whose efficiency in capturing this light depends on the R.I. of the surrounding medium. The closer the R.I. of the medium is to the core of the fibers, the more pronounced the coupling effect becomes. This property makes the sensor highly sensitive to variations in the surrounding R.I.

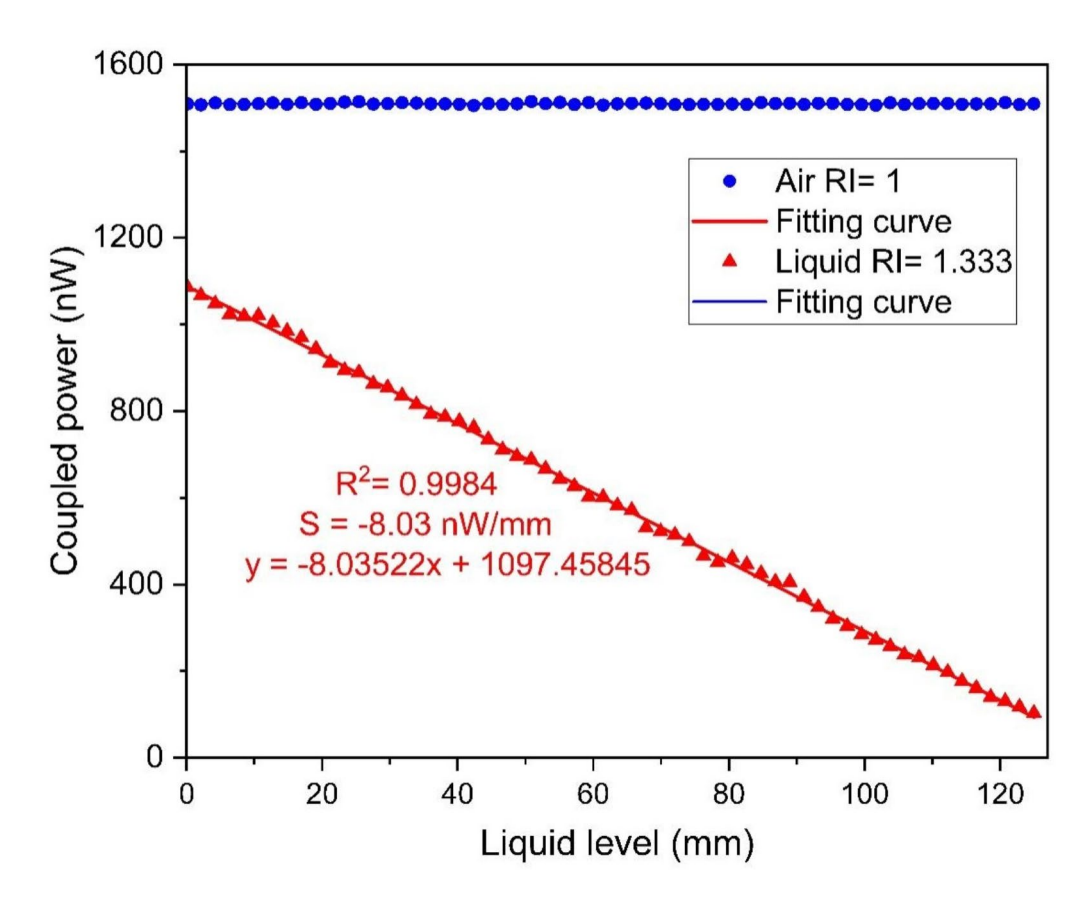


Fig. 4. Individually response of Liquid level sensor in air $(R.I. \approx 1)$ and ascending liquid level.

The sensor's ability to detect variations in R.I. is enhanced by the deliberate design of the coupling structure, which ensures that even small changes in the R.I. are captured by significant changes in the coupled power.

Although multimode optical fiber is nevertheless flexible enough to tolerate bending without significant loss, it also has downsides, which include signal latency distortions as well as scattering of light losses. Several methods were created to evaluate the macro-bending effects^{36,37}. To tackle these effects, ray tracing, beam propagation, finite element, and numerical aperture techniques are used. Nevertheless, both beam propagation and finite element techniques have constraints when it comes to attaining exceptional accuracy. On the other hand, the numerical aperture method is useless for optimization purposes. The ray-tracing method is advantageous since it requires low computational complexity and offers more precision compared to other methods. However, the proposed R.I. sensor sensitivity is based on TCMB technique, which can be optimized for a particular requirement. The optical configuration for measuring the R.I. is founded on the TCMB phenomenon.

In proposed setup, we designate an input port P_i for the incoming light. The twisted EF radiates light from the light source, while the AF relies on the coupling of power loss for light propagation. The output power of the EF at the throughput port is denoted as P_0 and the output power of the AF is referred to as the coupled port P_c . To illustrate the coupling power resulting from bend loss, we employ Eq. $(1)^{38}$:

$$P_c = \frac{1}{\sqrt{1 + \left(\frac{C \cdot nC}{\sqrt{2}}\right)^2}} \tag{1}$$

Here, P_c signifies the coupling power of the AF, n is the this represents the R.I. of fiber core, where C represents the coupling coefficient derived as per Eq. (2):

$$C = \frac{\sqrt{\frac{\delta}{U^2 K_0 \left[W\left(\frac{d}{\rho}\right)\right] V^3 K_1(W)}}}{\left(1 - \left(\frac{n_{cl}}{n_{co}}\right)^2\right)}$$
(2)

In this equation, $W\left(\frac{d}{\rho}\right)$ denotes the extent of isolation among the fibers, d represents the physical space of both coupled fibers, ρ denotes the core radius of the fibers, V is a dimensionless frequency defined as $V = U^2 + W^2$, U

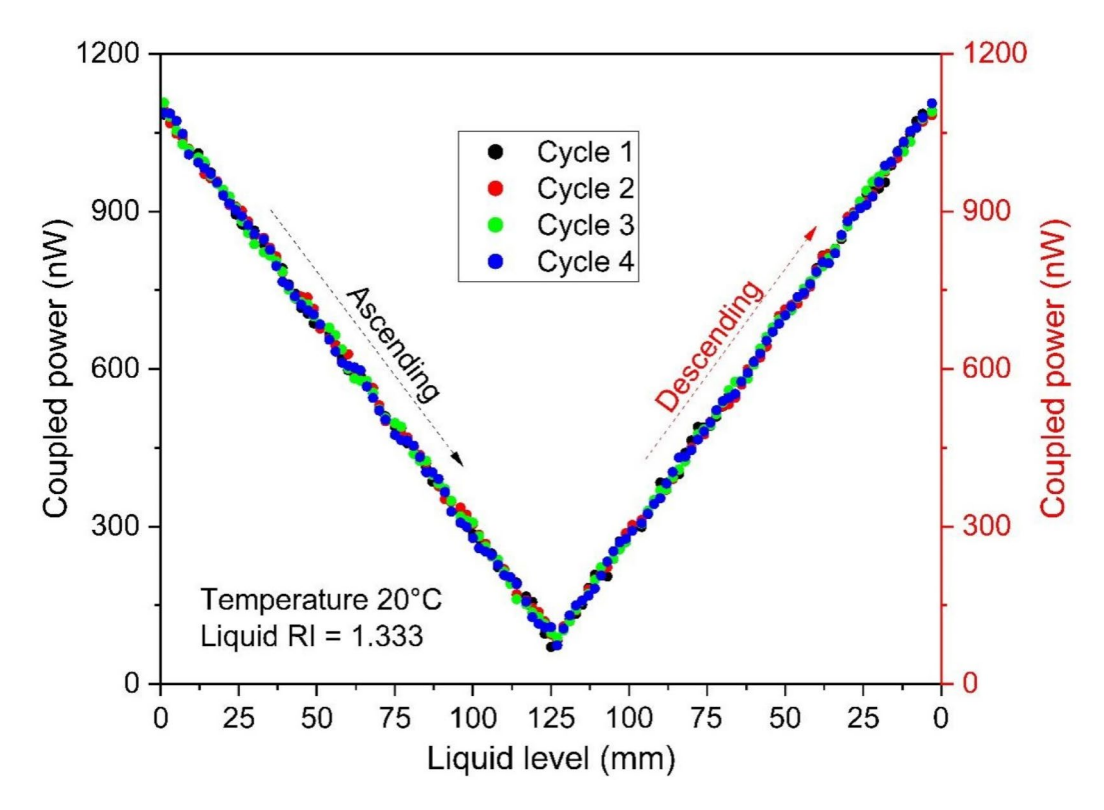


Fig. 5. The response of sensor to ascending and descending liquid level.

is the mode propagation in the fibers and K is Bessel function of the with specific indices of fiber. δ is defined as $\delta = 1 - \left(\frac{n_{cl}}{n_{co}}\right)^2$. where n_{cl} is R.I. of the fiber cladding and n_{co} is the R.I. of fiber core. Additionally, the coupling length l is determined by Eq. (3):

$$l = \frac{\pi P_c}{\sqrt{2nC}} \tag{3}$$

Experimental setup

The proposed method was experimentally implemented and fabricated for the simultaneous measurement of liquid level and R.I. The experimental setup utilizes three pieces of bare POF fiber. We specifically selected Mitsubishi Step Index SK-40 fiber for its elastic, soft, and flexible nature $^{39-41}$. The fiber has a diameter of 1000 μm , featuring a core diameter of 980 μm , and the cladding has 20 μm diameter, consisting of polymethylmethacrylate (PMMA) resin and a fluorinated polymer, and the core R.I. is 1.49. Notably, a larger core diameter and a smaller cladding area result in a significant bending loss from side coupling. The experimental arrangement involved using an LED light source (M660F1, Thorlabs) that operates at a wavelength of 660 nm, along with two photodetectors (S151C, Thorlabs), and they were attached to optical power meters (PM100USB, Thorlabs) connected to the front ends of the AFs to measure emitted energy. The schematic representation of the experimental setup is illustrated in Fig. 2.

Two AFs were twisted separately on the EF to achieve dual-parameter functionality from a single EF. The first twisting was terminated upon completion of the first loop and affixed to a vernier caliper depth meter secured with glue. The front end of the first AF was coupled to power meter 1, ensuring stable measurement conditions. Simultaneously, the other twisting fiber commenced with its front end-point coupled with power meter 2. The distance between the untwisted EF, from the point where the liquid level sensor ended to the point where the R.I. sensor began, was 50 cm. For liquid sensing, the twisting length was 125 mm, with a total length of 1 m to the power meter. For R.I. sensing, we used a 60 mm twisting length with a circular macro-bending region with the bending radius of 8 mm, also with a total length of 1 m to the power meter.

The liquid level sensor measurement apparatus utilized in this study consisted of a twisted and coupled OFS affixed to depth measurement tool of a vernier caliper with a maximum length of 150 mm, positioned perpendicularly above the liquid surface. To ensure the initial liquid level position remained stable, the sensor was slowly submerging into the liquid, which cover a range from 0 to 125 mm, in order to obtain accurate depth readings. The R.I. measurement employed the TCMB method, as depicted in Fig. 1c, where light from the visible-light source traversed through the first twist before the second twist commenced to fabricate the sensing region for R.I. sensing. The end point of the twisted AF was connected to the power meter for R.I. sensing. Sodium chloride solutions (NaCl) with varying concentrations were tested for their values using an Abbe refractometer,

Liquid level sensor	Level ascent sensitivity (nW/mm)	Correlation coefficient (R ²)	Level descent sensitivity (nW/mm)	Correlation coefficient (R ²)
Cycle 1	8.03	0.9982	8.03	0.9976
Cycle 2	7.96	0.9980	8.01	0.9985
Cycle 3	8.00	0.9983	8.04	0.9988
Cycle 4	8.01	0.9977	8.03	0.9986

Table 1. The results from Fig. 5.

yielding respective liquid R.I. values of 1.333, 1.340, 1.348, 1.353, and 1.361 for concentrations of 1 Mol/L, 1.5 Mol/L, 2 Mol/L, and 2.5 Mol/L, respectively, at room temperature 20 °C. The relationship between the liquids RI and the concentration of a NaCl solution is described using a linear equation known as the Gladstone-Dale Eq. (4):

$$R = \sqrt{A + \frac{B}{\left(S - C\right)^2}}\tag{4}$$

where *R* is the R.I. of the solution, *S* is the NaCl concentration mol/L, A, *B*, and *C* are constants specific to the solvent and the solute.

Results and discussion

The experiments were conducted for liquid level and R.I. measurement using the developed experimental platform to demonstrate the practicality of the POF-based liquid level and R.I. sensor. Figure 3, presents the initial response of both sensors, illustrating their performance individually in the liquid with an (RI=1.333). The coupling power in both sensors remains relatively steady when exposed in the environment. The POF sensor's steady response in air (R.I. \approx 1) is due to the large contrast between the air and the fiber core (SK 40 core RI=1.49), which ensures efficient light confinement within the core through total internal reflection. This contrast minimizes external disturbances and losses, maintaining a stable and consistent coupling power. Conversely, when ascended in a liquid with a higher refractive induces, then reduced contrast leads to increased coupling power loss and a more variable sensor response.

Sensor 1

The liquid level sensor can detect depths of 125 mm, which corresponds to the total length of the twisted coupled fibers. This range allows the sensor to cover every measurement point as the liquid level either ascends or descend. Figure 4, depicts the sensor's response to the liquid level in both air (R.I. \approx 1) and liquid (R.I. = 1.333) at a temperature of 20 °C. As the liquid level changes, the coupled power with continuous level changing and coupled power decreases linearly. Although, there is not such change in the air with the regression is settled at (R²=0.9989). Therefore, the sensitivity is derived by subtracting the initial power coupling from the final coupled power loss and then dividing this difference by the change in liquid level which drive as Eq. (5):

Sensitivity (nW/mm) =
$$\frac{P_f - P_i}{L_{max}}$$
 (5)

where P_f denotes the final power coupling, P_i signifies the initial power coupling, and L_{max} represents the variation in the liquid level. According to the equation, it is evident that the coupling power exhibits an approximate linear decreasing in coupled power loss trend with an ascent in the liquid level. The sensitivity of 8.03 nW/mm was obtained for liquid level sensing.

Moreover, the four cycles of ascent and descent of the liquid level sensor are illustrated in Fig. 5. The rate of level change is 2.08 mm/sec, with a measurement range extending to maximum. The experimental results are presented in Table 1. It shows that a sensitivity with a mean value of 8.00 ± 0.03 nW/mm level ascending, and for the level descending 8.03 ± 0.01 nW/mm. This precise control allows for accurate monitoring of liquid levels within the specified range. In the AF, a minimal coupled power loss occurs, which radiates at every level, ensuring a consistent small amount of propagated power through coupling with the EF. The coupling power loss varies with continuous change in liquid levels, crucial for real-time monitoring applications. The variation in coupling power loss corresponds to the continuous increase or decrease in the liquid levels. As depicted in Fig. 5, the coupled power loss increases during the ascending of the liquid level due to an increase in transmission loss. Conversely, during the descending of the coupled power increases, as shown in Fig. 5.

The temperature significantly impacts the sensor's performance. The PMMA POF is sensitive to temperature, while the SK-40 fiber has a specified temperature ranging from $-55\,^{\circ}\text{C}$ to 70 °C as per the manufacturer's specifications. A comprehensive analysis of temperature dependence was conducted on the sensor design to evaluate its performance in various environmental conditions shown in Fig. 6. The liquid level sensor was ascended and descended into liquid with an (R.I.=1.333) and the beaker was positioned on a Kaisi 818 heating apparatus, where the temperature varied between 20 °C and 60 °C at intervals of 20 °C. The results shown in Fig. 6, The decrease in output power with increasing temperature can be attributed to variations in the liquid's R.I., leading to weakened containment of light rays and some shifting into radiation mode, causing a decrease in power output.

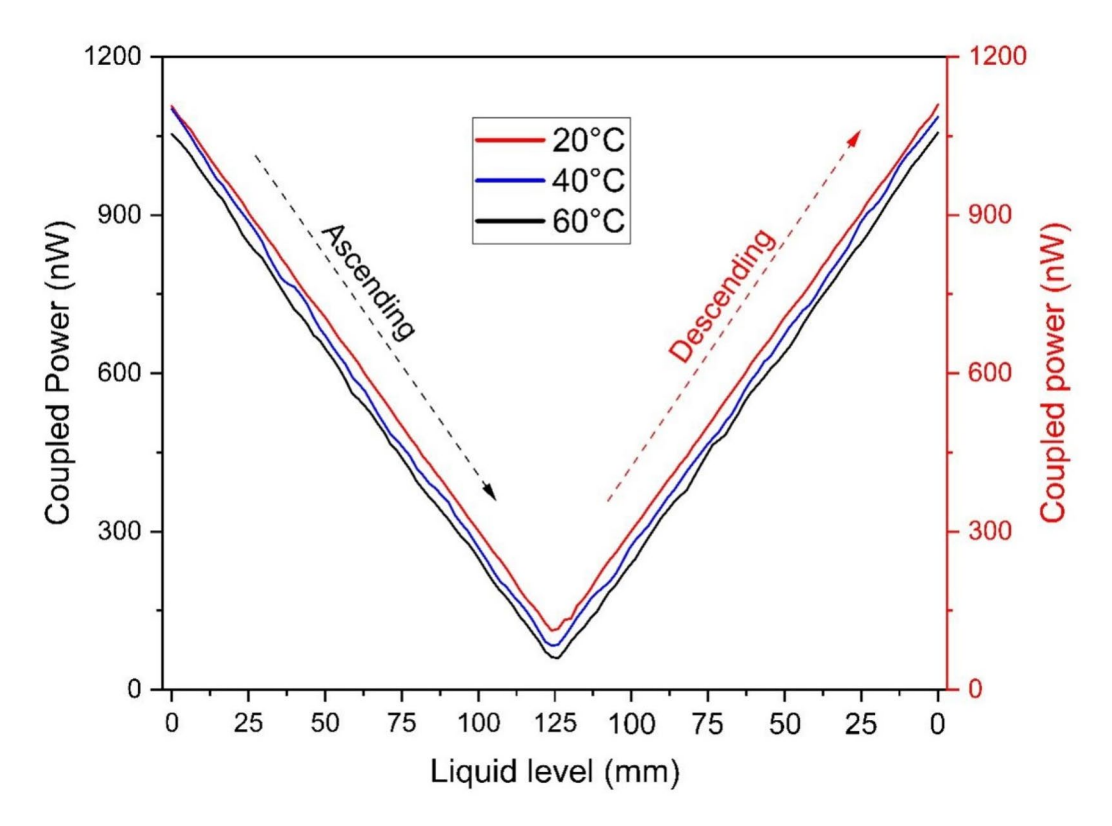


Fig. 6. Liquid level sensor ascended and descanted in liquid with different temperature °C.

Sensor 2

The sensor 2 is designated for R.I. sensing. The optical fiber setup consists of initially the twisted coupling configuration for sensor 1, then followed by TCMB technique for sensor 2. Sensor 1 maintains the highest power output, while there is a gradually decrease in power for the sensor 2. It should be emphasized that as more sensors are added to the EF, the initial power coupling diminishes when more sensors are added. The R.I. sensors demonstrate with exponential response attributed to the macro-bend loss effect. Figure 7. shows the different R.I. liquids sensing without TCMB effect and with TCMB effect. This TCMB technique exhibits a high of linearity, with a correlation coefficient (R²) 0.99774 and increased sensitivity in comparison to not using TCMB technique. The TCMB effect induces more coupling power loss for the R.I. sensor, thereby increasing its sensitivity to even minor variations in the R.I. Having considered this, we have analyzed different bending radii to evaluate their influence on sensor functionality as shown in Fig. 8.

The TCMB design is dependent on macro-bending sensing, leading to the transformation of a fiber's core mode into a radiation mode once it reaches a specific threshold of the bending radius. At this point, the fiber experiences macro-bend radiation loss. This can cause more of the light to escape from the core into the cladding, increasing interaction with the surrounding medium. Increased refraction at the boundary between the central region and the outer layer in an optical fiber leads to the emission of some incident light from the EF. In multimode fibers with extremely small bending radii, the light loss at the core-cladding boundary is insignificant as a grated amount of power is directed towards the cladding, resulting in the creation of a significant cladding mode. Figure 8. demonstrates the impact of various bending radii on the operational behavior of the sensor. As the radius decreases, the fiber experiences increased bending loss. The analysis revealed that sensitivity is enhanced with smaller bend radii 8 mm, leading to greater radiant illumination surrounding the bend area and improved coupling of light in the AF. The radiated power can be determined with the equation $P_r = P_0 \times T$, where P_0 represents the baseline intensity within the EF, T signifies the Fresnel transmission coefficient, while P_r represents light intensity that escapes the field⁴². The sensitivity comparison of the R.I. sensor is shown in Table 2.

Liquid level and RI simultaneous response

To evaluate the proposed sensor's simultaneously measuring capability for liquid level and R.I., we submerged the liquid level sensor to the maximum depth of 125 mm in a liquid with (RI = 1.333), and then placed the R.I. sensor in liquids with different NaCl saturated liquids shown in Fig. 9. When the maximum coupling power loss occurred at the maximum liquid level depth, the sensitivity of -2624%/RIU was achieved by the R.I. sensor, which had a resolution of 3.810×10^{-4} in different NaCl liquids simultaneously without any interference between the two measurements. The R.I. sensor's correlation coefficient was 0.99827, and although a slight additional

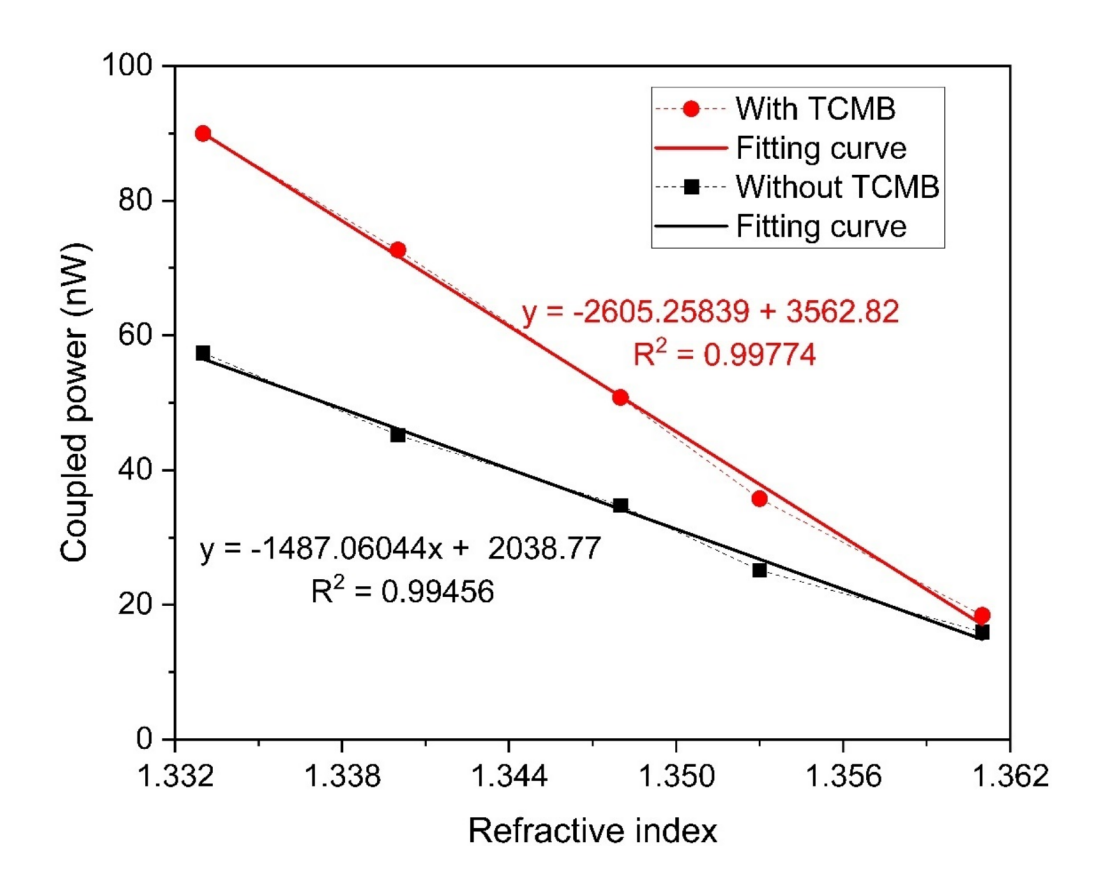


Fig. 7. Response of R.I. sensor with and without TCMB technicities in different NaCl saturated liquid.

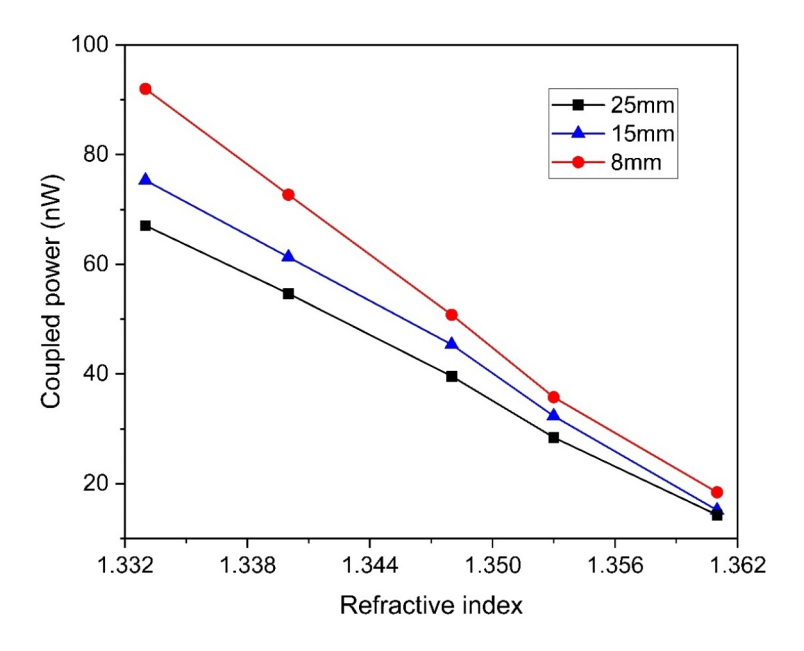


Fig. 8. R.I. sensor response at different bending radii.

TCMB Radius (mm)	Sensitivity (%/RIU)	Resolution (RIU)	Correlation coefficient (R ²)	Y = ax + b
25	-1906	5.246×10 ⁻⁴	0.99897	-1906.09666x + 2608.3297
15	-2158	4.632×10^{-4}	0.99818	-2158.75279x + 2953.7499
8	-2663	3.754×10^{-4}	0.99740	-2663.83579x + 3642.1256

Table 2. Sensitivity response with different TCMB radii.

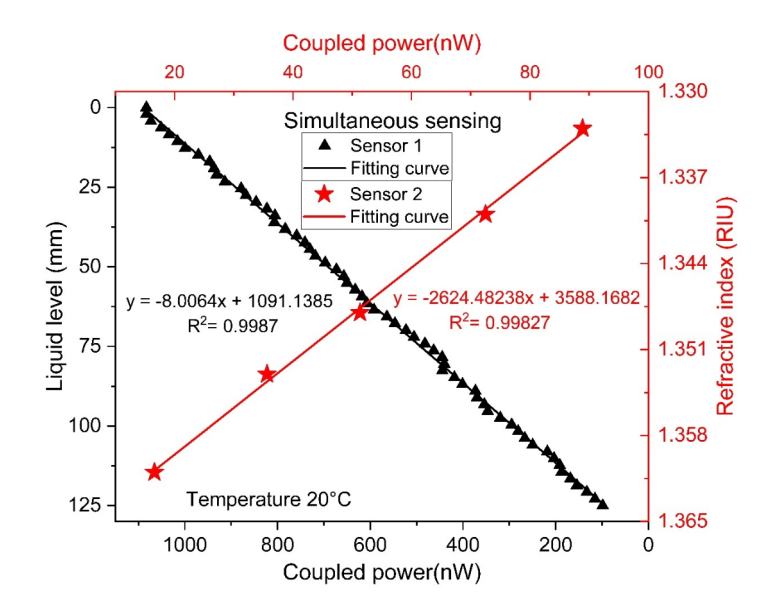


Fig. 9. Simultaneous response of both sensors as the liquid level sensor was ascended to its maximum depth and the R.I. sensor measured the different NaCl-saturated liquids.

References	Method	Parameter	Liquid level sensitivity	R.I. sensitivity	Range of detection
24	Micro-holes	Liquid level	-	-	0-550 mm
25	Twisted tapering	Liquid level	0.65%/mm	-	0-23 mm
26	Tapering	R.I.	-	107dB/RIU	1.333-1.410
27	MMI	Liquid level & R.I.	532pm/mm,	875pm/mm	1.3335-1.4164
29	Side-polishing, bending	R.I.	-	57 uW/ RIU	1.333-1.455
30	SPR	Liquid level & R.I.	0.00755 /mm	2024.41 nm/RIU	0-25 mm 1.335-1.40
31	MZI	Liquid level & R.I.	0.88n/mm	315.21 nm/RIU	0-30 mm 1.3296-1.3564
33	Micro-holes	Liquid level & R.I.	0.029%/mm	-22.8%/RIU	0–90 mm 1.333 to 1.475
34	U-shaped notch	Liquid level & R.I.	0.059%/mm	107.6 ± 4.4%/RIU	0-120 mm 1.333-1.443
This work	TCMB	Liquid level & R.I.	8 nW/mm	-2663%/RIU	0–125 mm 1.333–1.361

Table 3. The comparison between the purposed sensor with other liquid level and R.I. sensors.

power loss was observed in the R.I sensor, it was negligible and did not affect the response of both sensors operating simultaneously.

The liquid level and R.I. sensors described in the literature are compared with the proposed OFSs, as illustrated in Table 3. The proposed sensor can be readily manufactured, requiring only twisting and macrobending, without additional treatments such as tapering, side polishing, or Bragg grating. Multiparameter sensing of liquid level and R.I. is made possible by this sensor. The liquid level sensor exhibits a sensitivity of 8 nW/mm as shown in Fig. 9. Simultaneously R.I sensor measurements demonstrate a sensitivity of -2663%/ RIU with a resolution of 3.754×10^{-4} RIU. The developed sensor maintains good consistency and reliability, and

the experimental results showing its stability as a multi-parameter sensor. This sensor can find applications in various industrial and commercial sectors, including chemical, petroleum, pharmaceutical industries and more.

Conclusion

This paper presents a sensor system that can simultaneously measure liquid level and R.I. using POF. The sensor employs a twisted structure and coupling phenomenon for liquid level sensing, and a TCMB approach for R.I. sensing. The multiparameter sensor structure couples the light from single source to an EF, while the AFs are connected to a two different power meters to measure the coupled power intensity. This sensor operates on the principle of coupling power loss phenomenon. The sensor is analyzed using two configurations: a straight twisted fiber for liquid level measurement and a micro-bent fiber for R.I. measurement. It was observed that the straight coupled fiber did not exhibit any significant change, so a twisting coupled structure was established. The twisted structure was evaluated under conditions with and without bending for the R.I. sensing. It was noticed that the bend radius had an influence on the R.I. sensing, where a smaller bending radius exhibited higher sensitivity and increasing the radius resulted in lower sensitivity. The coupling length is an important factor, as a longer twisted-coupling length leads to more coupled power. Finally, intensity-based scheme working on coupling power loss is adopted to achieve a multi-parameter liquid level and R.I. sensing.

Data availability

The data is available on demand from the corresponding author.

Received: 29 July 2024; Accepted: 30 December 2024

Published online: 07 January 2025

References

- 1. Chen, Y., Li, C. & Yang, X. Simultaneous measurement of trace dimethyl methyl phosphate and temperature using all fiber Michaelson interferometer cascaded FBG. Opt. Express 31(4), 6203–6216 (2023).
- 2. Liu, P. Y. et al. Cell refractive index for cell biology and disease diagnosis: Past, present and future. Lab. Chip 16(4), 634-644 (2016).
- 3. Ghaffar, A. et al. Multiplexing sensors technique for angle and temperature measurement using polymer optical fiber. *Infrared Phys. Technol.* **130**, 104585 (2023).
- 4. Pereira, L. et al. Compact dual-strain sensitivity polymer optical fiber grating for multi-parameter sensing. *J. Lightwave Technol.* **39**(7), 2230–2240 (2021).
- 5. Kong, L. et al. Lab-in-fibers: Single optical fiber with three channels for simultaneous detection of pH value, refractive index and temperature. Sens. Actuators B 385, 133727 (2023).
- Huang, Y. et al. Simultaneous detection of liquid level and refractive index with a long-period fiber grating based sensor device. Meas. Sci. Technol. 24 (9), 095303 (2013).
- 7. Wang, J. et al. A novel method for integrity assessment of soil-nailing works with actively heated fiber-optic sensors. J. Geotech. GeoEnviron. Eng. 150(8), 04024063 (2024).
- 8. Shi, J. et al. Dynamic rotational sensor using polymer optical fiber for robot movement assessment based on intensity variation. *Polymers* 14. https://doi.org/10.3390/polym14235167 (2022).
- 9. Chen, B., Hu, J. & Ghosh, B. K. Finite-time tracking control of heterogeneous multi-AUV systems with partial measurements and intermittent communication. Sci. China Inform. Sci. 67(5), 152202 (2024).
- 10. Teng, C. et al. Intensity-modulated polymer optical fiber-based refractive index sensor: A review. Sensors 22. https://doi.org/10.33 90/s22010081 (2022).
- 11. Roldán-Varona, P. et al. Liquid level sensor based on dynamic fabry-perot interferometers in processed capillary fiber. Sci. Rep. 11 (1), 3039 (2021).
- 12. de Oliveira, H. J. B. et al. Refractive index sensors based on cascaded multimode interference hetero-core optical fibers. *Appl. Opt.* **62**(16), E16–E23 (2023).
- 13. Wang, G. & Feng, W. On-chip Mach-Zehnder interferometer sensor with a double-slot hybrid plasmonic waveguide for high-sensitivity hydrogen detection. *Opt. Express* 31(24), 39500–39513 (2023).
- 14. Chamoli, S. K. Long period grating in a liquid crystal waveguide. *Optik* **201**, 163482 (2020).
- 15. Shao, M. et al. Liquid level sensor using fiber Bragg grating assisted by multimode fiber core. *IEEE Sens. J.* **16** (8), 2374–2379 (2016)
- Pendão, C. & Silva, I. Optical Fiber sensors and sensing networks: Overview of the main principles and applications. Sensors 22. https://doi.org/10.3390/s22197554 (2022).
- 17. Roriz, P. et al. Fiber optic intensity-modulated sensors: A review in biomechanics. Photonic Sens. 2(4), 315-330 (2012).
- 18. He, Y. et al. Accuracy characterization of Shack–Hartmann sensor with residual error removal in spherical wavefront calibration. *Light: Adv. Manuf.* 4(4), 393–403 (2024).
- 19. Du, W. & Wang, G. Fully probabilistic seismic displacement analysis of spatially distributed slopes using spatially correlated vector intensity measures. *Earthq. Eng. Struct. Dyn.* **43**(5), 661–679 (2014).
- 20. Hussian, S. et al. Development of a dual point humidity sensor using POF based on twisted fiber structure. Sci. Rep. 14(1), 10735 (2024).
- 21. Ghaffar, A. et al. High pressure sensor based on intensity-variation using polymer optical fiber. Sci. Rep. 14(1), 18604 (2024).
- Dong, Y. et al. An Optical liquid-level sensor based on D-shape fiber modal interferometer. IEEE Photonics Technol. Lett. 29(13), 1067–1070 (2017).
- 23. Zhang, Y. et al. A multipoint liquid level sensor based on two twisted polymer optical fibers in a race-track helical structure. *J. Sens.* **2018**, 1–4 (2018).
- 24. Park, J., Park, Y. J. & Shin, J. D. Plastic optical fiber sensor based on in-fiber microholes for level measurement. *Jpn. J. Appl. Phys.* 54(2), 028002 (2015).
- 25. Deng, S. et al. Twisted tapered plastic optical fibers for continuous liquid level sensing. Opt. Fiber. Technol. 59, 102318 (2020).
- 26. Ujihara, H. et al. Polymer optical fiber tapering without the use of external heat source and its application to refractive index sensing. Appl. Phys. Express 8(7), 072501 (2015).
- 27. Chen, Q. et al. A liquid level optical fiber sensor with refractive index compensation through cascading double multi-mode interferences. *Infrared Phys. Technol.* 127, 104437 (2022).
- 28. Jing, N. et al. Refractive index sensing based on a side-polished macrobending plastic optical fiber. IEEE Sens. J. 15(5), 1-1 (2014).
- 29. De-Jun, F. et al. D-Shaped plastic optical fiber sensor for testing refractive index. *IEEE Sens. J.* 14(5), 1673–1676 (2014).

- 30. Teng, C. et al. Plastic optical fiber based SPR sensor for simultaneous measurement of refractive index and liquid level. IEEE Sens. J. **22**(7), 6677–6684 (2022).
- 31. Yang, X. et al. Simultaneous measurement of liquid level and refractive index based on a sandwich multimode optical fiber structure. Opt. Laser Technol. 168, 109856 (2024).
- 32. Chuanxin, T. et al. Simultaneous measurement of refractive index and temperature based on a side-polish and V-groove plastic optical fiber SPR sensor. Opt. Lett. 48(2), 235-238 (2023).
- 33. Ye, Y. et al. Portable multihole plastic optical fiber sensor for liquid-level and refractive index monitoring. IEEE Sens. J. 23(3), 2161-2168 (2023).
- 34. Zhao, C. et al. Notch POF integrated with smartphone for liquid level and refractive index monitoring. Opt. Laser Technol. 167, 109751 (2023)
- 35. Agarwal, A. K. Review of optical fiber couplers. Fiber Integr. Opt. 6(1), 27-53 (1987).
- 36. Kamizi, M. A. et al. Multiplexing optical fiber macro-bend load sensors. J. Lightwave Technol. 37(18), 4858-4863 (2019).
- 37. Zhang, Z. F. et al. Dependence of macro-bending loss on bending configuration of multimode optical fibers studied by ray-tracing simulation. Opt. Rev. 27(3), 290-295 (2020).
- 38. Snyder, A. W. Coupled-mode theory for optical fibers. JOSA 62(11), 1267-1277 (1972).
- 39. Ghaffar, A. et al. A simple and high-resolution POF displacement sensor based on face-coupling method. Measurement 187, 110285 (2022).
- 40. Specification sheet of high-performance plastic optical fiber. Mitsubishi Rayon Co., LTD 6-41 konan 1-chome, minato-ku, Tokyo,
- 41. Hu, Y. et al. A narrow groove structure based plasmonic refractive index sensor. IEEE Access 8, 97289-97295 (2020).
- 42. Bahin, L. et al. Smart textiles with polymer optical fibre implementation for in-situ measurements of compression and bending. Sens. Actuators A: Phys. 350, 114117 (2023).

Acknowledgements

This Research was Supported by the National Natural Science Foundation of China under Grant 61901065, and in part by the Natural Science Foundation of Chongqing under Grant cstc2021jcyj-msxmX0480.

Author contributions

Formal analysis, Sadam Hussain, Mujahid Mehdi and Laraib Unsa Noor; Funding acquisition, Chen Chen and Min Liu; Investigation, Sabir Ali Kahoro and Laraib Unsa Noor; Methodology, Muhammad Saleh Urf Kumail Haider, Sabir Ali Kalhoro and Abdul Ghaffar; Validation and Review, Chen Chen, Abdul Ghaffar, and Min Liu; Writing - original draft Muhammad Saleh Urf Kumail Haider.

Declarations

Competing interests

The authors declare no competing interests.

Additional information

Correspondence and requests for materials should be addressed to C.C. or A.G.

Reprints and permissions information is available at www.nature.com/reprints.

Publisher's note Springer Nature remains neutral with regard to jurisdictional claims in published maps and institutional affiliations.

Open Access This article is licensed under a Creative Commons Attribution-NonCommercial-NoDerivatives 4.0 International License, which permits any non-commercial use, sharing, distribution and reproduction in any medium or format, as long as you give appropriate credit to the original author(s) and the source, provide a link to the Creative Commons licence, and indicate if you modified the licensed material. You do not have permission under this licence to share adapted material derived from this article or parts of it. The images or other third party material in this article are included in the article's Creative Commons licence, unless indicated otherwise in a credit line to the material. If material is not included in the article's Creative Commons licence and your intended use is not permitted by statutory regulation or exceeds the permitted use, you will need to obtain permission directly from the copyright holder. To view a copy of this licence, visit http://creativecommo ns.org/licenses/by-nc-nd/4.0/.

© The Author(s) 2025